

Observation of space-time nonseparable helical pulses

Ren Wang^{1,2*}, Shuai Shi¹, Zeyi Zhang¹, Bing-Zhong Wang¹, Nilo Mata-Cervera^{3,4},
Miguel A. Porras³, Yijie Shen^{4,5,6*}

¹ *Institute of Applied Physics, University of Electronic Science and Technology of China,
Chengdu 611731, China*

² *Yangtze Delta Region Institute (Huzhou), University of Electronic Science and
Technology of China, Huzhou 313098, China*

³ *Grupo de Sistemas Complejos, ETSIME, Universidad Politécnica de Madrid, Rios
Rosas 21, 28003 Madrid, Spain*

⁴ *Centre for Disruptive Photonic Technologies, School of Physical and Mathematical
Sciences, Nanyang Technological University, Singapore 637371, Singapore*

⁵ *School of Electrical and Electronic Engineering, Nanyang Technological University,
Singapore 639798, Singapore*

⁶ *International Institute for Sustainability with Knotted Chiral Meta Matter (WPI-
SKCM2), Hiroshima University, Hiroshima 739-8526, Japan*

* E-mail: rwang@uestc.edu.cn (R.W); yijie.shen@ntu.edu.sg (Y.S.)

Abstract

Chirality is a fascinating natural phenomenon with widespread applications in scientific research. Toroidal responses, distinct from chiral responses, represent an emerging and intriguing field that investigates toroidal electromagnetic phenomena. This field has garnered significant attention following the first experimental observations of oscillating toroidal dipoles and electromagnetic toroidal pulses. Breaking the symmetry of toroidal responses and observing chiral toroidal responses are crucial for advancing our understanding of toroidal phenomena and expanding the theoretical and practical applications of toroidal electrodynamics. Here, we present two complementary methods for breaking the symmetry of toroidal pulses and generating chiral space-time nonseparable helical pulses (SNHPs)—quasi-linearly polarized and chiral toroidal—across the optical and microwave spectral ranges. This was achieved through polarization decomposition of toroidal light pulses and direct emission from an ultrawideband spiral antenna, respectively. These advancements pave the way for experimental investigations into information transfer and light-matter interactions involving chiral SNHPs, including toroid-vortex coupling, classical-quantal entanglement, and optical machining, all of which are of growing interest in both fundamental science and practical applications.

Introduction

Chiral responses and toroidal responses are two distinct fundamental natural phenomena. Chirality, which occurs when an object cannot be made to coincide with its mirror image through simple translation or rotation, has wide-ranging implications in scientific research [1–10]. This inherent asymmetry is crucial in various fields, influencing processes such as information and energy transfer, precision measurement, and the interaction between waves and matter [11-20].

Toroidal electrodynamics is an emerging field focused on the research of toroidal electromagnetic phenomena, which has gained significant attention since the first experimental observations of oscillating toroidal dipoles in 2010 [21] and electromagnetic toroidal pulses in 2022 [22]. Toroidal responses have been identified as significant contributors to the linear and nonlinear optical properties of materials [23]. This has led to the development of new spectroscopic techniques based on toroidal effects [24], and the exploration of non-radiating anapoles—special configurations where electric and toroidal dipoles co-exist—has captured increasing attention [25]. Toroidal pulses, known for their non-transverse skyrmion topological structures [26-27], space-time nonseparability [28, 29], and strong matter interactions [23, 30], have been successfully generated in the optical, terahertz, and microwave domains [22, 31-32]. These developments have paved the way for applications like superresolution positioning [33], spurring a new wave of research into this novel form of structured light. Nevertheless, the toroidal excitations observed so far in free space generally

exhibit rotational symmetry. Breaking this symmetry to achieve chiral toroidal responses is crucial for advancing understanding of toroidal phenomena and expanding the theoretical and practical boundaries of toroidal electrodynamics.

In this paper, we present two complementary methods for breaking the symmetry of toroidal pulses and generating chiral space-time nonseparable helical pulses (SNHPs) across the optical and microwave spectral ranges. Quasi-linearly polarized SNHPs are produced through the polarization decomposition of optical toroidal light pulses, while chiral toroidal SNHPs are directly emitted from a microwave ultrawideband spiral emitter.

Results

Derivation of SNHPs.

In 1985, Ziolkowski proposed an intriguing class of single-cycle space-time nonseparable structured electromagnetic solutions to Maxwell's equations, known as electromagnetic directed-energy pulse trains [34, 35]. In 1996, Hellwarth and Nouchi introduced toroidal pulses according to Ziolkowski's solution [36]. In 2004, Lekner theoretically introduced azimuthal dependence to Ziolkowski's solution [37], giving rise to a new pulse solution [38], i.e. the scalar SNHP solutions. These solutions are

given by $f(\mathbf{r}, t) = \left(\frac{\rho}{q_1 + i\tau}\right)^{\ell} e^{i\ell\theta} \frac{f_0}{(\rho^2 + (q_1 + i\tau)(q_2 - i\sigma))^\alpha}$, where $\mathbf{r} = [x \ y \ z]$, $x + iy = \rho e^{i\theta}$,

$\tau = z - ct$, $\sigma = z + ct$, f_0 is a normalizing constant, ℓ is an integer defining the topological number, $\alpha > 0$ is related to the energy confinement of the pulse, while

$\alpha \geq |\ell|$ leads to finite-energy pulses, $c = 1/\sqrt{\mu_0 \varepsilon_0}$ is the speed of light, and ε_0 and μ_0 are the permittivity and permeability of the medium, respectively. In this paper, we set the parameter $\alpha = 1$ and limit to $|\ell| = 1$. When compared to a Gaussian beam, the parameters q_2 and q_1 represent the Rayleigh range and the effective wavelength, respectively. The electric and magnetic fields of transverse electric (TE) pulses are represented by $\mathbf{E} = c^{-1} \partial_t \mathbf{A}$ and $\mathbf{B} = \nabla \times \mathbf{A}$, where \mathbf{A} is the Hertz potential. Transverse magnetic (TM) pulses can be obtained through the dual transformation $\mathbf{E} \rightarrow \sqrt{\mu_0 / \varepsilon_0} \mathbf{B} = \sqrt{\mu_0 / \varepsilon_0} \nabla \times \mathbf{A}$, $\mathbf{B} \rightarrow -\sqrt{\varepsilon_0 / \mu_0} \mathbf{E} = -\sqrt{\varepsilon_0 / \mu_0} \partial_t \mathbf{A}$ of TE pulses. Different SNHP fields can be derived using different Hertz potentials. For example, when the Hertz potential $\mathbf{A} = \nabla \times [f, 0, 0]$ is used, a quasi-linearly polarized SNHP can be obtained. In particular, self-dual SNHPs can be realized by combining TE and TM SNHPs. When the Hertz potential $\mathbf{A} = \nabla \times [-if, f, 0]$ is used, the field of self-dual SNHPs can form a chiral toroidal topology. Please see supplementary materials for details.

From the aforementioned two examples, one can see such SNHPs possess several interesting features: (1) SNHPs represent a class of space–time nonseparable solutions to Maxwell’s equations (see supplementary materials for details). This of SNHPs manifests in the space-spectrum domain as position-dependent frequency across the transverse plane, as illustrated by the amplitude propagation trajectories of different frequency components in Fig. 1(a). (2) SNHPs are single-cycle pulses. These pulses exist as short, localized bursts of radiation, each lasting for a single cycle. They possess

a broad spectrum and finite total energy, as illustrated in Fig. 1(a) (see supplementary materials for details). (3) SNHPs exhibit a family of spatiotemporal chiral helical topologies. Based on different Hertzian potentials, we derive several distinct types of helical pulses (see supplementary materials for details). These pulses can have different field components, each with its own unique topological structure. The helical topologies of these field components may be either identical or different. For example, Figs. 1(b) and 1(c) illustrate two kinds of SNHPs to be generated in the paper. (4) SNHPs can be non-transverse electromagnetic vortices. Conventional electromagnetic chiral vortices are typically transverse electromagnetic waves, with electric and magnetic fields oscillating perpendicular to the direction of propagation. However, some SNHPs can be non-transverse, exhibiting topological field vector structures that form chiral toroidal shapes, as shown in Fig. 1(c). Detailed derivation and analysis of these structures can be found in the supplementary materials. (5) SNHPs exhibit chiral helical singularity. In conventional electromagnetic vortices, singularities typically form along the central axis of propagation. However, in the case of SNHPs, the singularities can take on a double-helix shape and vortex-antivortex annihilation can occur during the propagation [39].

From the aforementioned characteristics, it is evident that SNHPs combine the distinctive features of both chiral vortices and toroidal pulses. They represent a new type of helical-shaped spatiotemporal wavepacket. However, such pulses have not yet been observed. Next, we will introduce methods for breaking the symmetry of toroidal

pulses and generating two kinds of SNHPs, i.e. quasi-linearly polarized SNHPs and chiral toroidal SNHPs.

Observation of quasi-linearly polarized SNHPs.

Quasi-linearly polarized SNHPs can be generated by utilizing polarization conversion surfaces to decompose optical toroidal pulses, as depicted in Fig. 1(b). The transverse electric field components of TM toroidal pulses distribute radially, with their unit vector denoted as e_r . These pulses can be decomposed into superpositions of left-handed and right-handed circularly polarized fields with topological charges ℓ and $-\ell$, respectively, i.e. $e_r = e^{-i\ell\varphi}e_R + e^{i\ell\varphi}e_L$. When passing through a circular polarizer, the left-handed or right-handed components can be separated. For instance, after passing through a left-handed circular polarizer, the emitted component can be expressed as $e^{-i\ell\varphi}e_R = e^{-i\ell\varphi}x + e^{i\ell\varphi}y$. When this component undergoes a linear polarizer, it can produce fields with topological charges ℓ or $-\ell$.

To validate the effectiveness of the above approach, we conducted experiments following the method shown in Fig. 1(b). We utilized TM optical toroidal pulses with $q_1=192$ nm and $q_2=75000q_1$ reported in [22] as the input light and employed a quarter-wave plate (QWP) and a polarizer to achieve circular and linear polarization decomposition, respectively. Subsequently, we analyzed the vortex nature of the generated waves through edge diffraction patterns (please see supplementary materials for details). In the absence of an opaque edge, the CCD camera detected the intensity

distribution of light at different wavelengths, shown in Fig. 2(a). It was observed that the intensities exhibited ring-shaped distributions at all wavelengths, consistent with the intensity distribution of SNHPs. In the presence of an opaque edge, diffraction patterns observed by the experimental system are depicted in Fig. 2(b), displaying distinct fork-shaped pattern at each wavelength, indicating the presence of optical vortices consistent with those of SNHPs. For comparison, when the aforementioned polarization decomposition lenses were absent, the diffraction patterns of toroidal pulses observed by the experimental system showed no vortex phenomenon (details in the supplementary materials).

In addition to the vortex field distribution, another important characteristic of SNHPs is their space-time inseparability, where the propagation trajectories of different wavelength components exhibit isodiffraction properties [29]. The concurrence $con = \sqrt{2[1 - Tr(\rho_A^2)]}/\sqrt{2(1 - 1/n)}$ and entanglement of formation $EoF = -Tr[\rho_A \log_2(\rho_A)]/\log_2(n)$, where n and ρ_A are the state dimension and the reduced density matrix [40], respectively, as shown in Fig. 2 (c), remain above 0.9 with distance, indicating a good space-time nonseparability. The measured tracking curves of the maximum field positions for different wavelengths in (c) show that the trajectories of different wavelengths do not cross when the incident wave is a toroidal pulse, demonstrating isodiffraction characteristics. The measured state-tomography matrix $\{c_{i,j}\}$ in Fig. 2(d) is diagonalized, indicating strong isodiffraction characteristics, where $c_{i,j} = \int \varepsilon_{\eta_i} \varepsilon_{\lambda_j}^* dr$ represents the overlap of spatial and spectral states and. Here, ε_{λ_j} and

ε_{η_i} describe the distributions of monochromatic energy density and total energy density [29], respectively. The measured fidelity $F = \text{Tr}(M_1 M_2)$ [41], where M_1 and M_2 are the density matrices for the generated and canonical SNHPs, exceeds 0.8, indicating a good match with canonical SNHPs. For comparison, as shown in the supplementary materials, when the incident wave is a radially polarized Gaussian beam, the spectral tracking curves of the generated pulses exhibit crossing behavior and the measured state-tomography matrix appears disordered, indicating poor spacetime nonseparability and a poor match with canonical SNHPs. The comparison manifests the spacetime nonseparability of generated SNHPs can be inherited from incident toroidal pulses.

In summary, employing polarization decomposition methods allows for the transformation of incident toroidal pulses into SNHPs. Furthermore, as analyzed earlier, altering the rotation direction of the circular polarizer enables the generation of SNHPs with opposite chirality (details in the supplementary materials).

Observation of chiral toroidal SNHPs.

We generated chiral toroidal SNHPs in the microwave frequency range using a dual-arm spiral antenna, as shown in Fig. 1(c). The spiral structure, though extensively employed in the creation of optical vortexes and various structural light configurations [42-48], has, interestingly, not been documented in its application towards generating SNHPs. This gap in research presents an intriguing opportunity to explore the potential of spiral structures in generating such fascinating pulses. The spiral emitter used in this

study operates within a frequency band of 1.5-8.5 GHz, covering the main frequency range of the chiral toroidal SNHP with parameters $q_1 = 0.03$ m, $q_2 = 20q_1$, and $\ell=1$, as shown in Figs. 3(a1-a3). The spiral emitter is fed by a signal calculated according to the canonical SNHP and the response of the spiral emitter through a coaxial connector (see supplementary materials for details). By altering the rotation direction of the spiral, SNHPs with opposite chirality can be produced. The spiral emitter's substrate lacks a ground plane on its backside, which is crucial for generating SNHPs, as ground reflections would disrupt their structure. Typically, microwave spiral antennas incorporate a ground plane on the backside to achieve unidirectional radiation, making it difficult to observe SNHPs (see supplementary materials for details).

We measured the SNHPs generated by the spiral emitter using a microwave anechoic chamber and a planar near-field measurement system. Details of the measurement setup and method can be found in the supplementary materials. Spatial frequency spectra of canonical, simulated, and measured E_y components of the SNHPs are depicted in Figs. 3(a1-a3). Both the simulated and measured SNHPs exhibit a wide bandwidth, with the spatial spectrum narrowing as the frequency increases and the maximum moving closer to the central axis $\rho = 0$. This behavior is consistent with that of the canonical SNHPs. Fig. 3(a3) highlights the maximum positions of each frequency point in the spatial spectra of the canonical, simulated, and measured SNHPs, demonstrating similar trends. The spatial spectra of the E_x and E_z components of the canonical, simulated, and measured SNHPs also follow similar patterns (see supplementary materials for details).

The spatiotemporal field distributions of the transverse component E_y and longitudinal component E_z for the canonical, simulated, and measured SNHPs are shown in Figs. 3(b1-b3) and (c1-c3), respectively. Both the simulated and measured E_y components exhibit a double-lobe single-cycle helical topology similar to that of the canonical SNHPs. Similarly, the simulated and measured E_z components display a four-lobe helical topology akin to the canonical SNHPs. The spatiotemporal field distribution of another transverse component E_x for the canonical, simulated, and measured SNHPs is also similar to the single-cycle helical topology observed in the E_y component distributions shown in Figs. 3(b1-b3) (see supplementary materials for details).

We evaluated the isodiffraction characteristic of SNHPs, which is related to space-time nonseparability, to assess how it evolves after radiating from the spiral emitter. The concurrence and entanglement of formation corresponding to the measured transverse electric field components E_x and E_y of SNHPs, respectively shown in Figs. 3 (d1) and (d2), quickly increase and remain above 0.8 with distance. During propagation, the experimentally generated pulses evolve towards stronger space-time nonseparability, similar to the resilient propagation characteristic of toroidal pulses [32]. The measured state-tomography matrix of E_x and E_y of the generated chiral toroidal SNHPs are inserted in Figs. 3(d1) and (d2), respectively. The measured state-tomography matrices are nearly diagonal, indicating good spatiotemporal nonseparability. The measured fidelities exceed 0.8, suggesting a relatively good match with canonical chiral toroidal

SNHPs. The trajectories of different frequencies also demonstrate the space-time nonseparability of the generated SNHPs (see supplementary materials for details). In conclusion, employing a spiral emitter allows for the generation of SNHPs.

Conclusions

We have demonstrated the generation and detection of two distinct types of chiral SNHPs across the optical and microwave spectral regions, elucidating their topological characteristics and inherent space-time nonseparability. Such pulses are fundamental exact solutions of Maxwell's equations, incorporating distinctive features of chiral vortices and toroidal pulses.

The chiral toroidal oscillation is now demonstrated to exist in the form of bursts of electromagnetic energy propagating in free space. This revelation offers exciting prospects for novel light-matter interactions. The single-cycle spatiotemporal chiral nature of SNHPs holds significant potential for investigating transient and nonlinear physics. Moreover, the non-transverse nature and diverse topologies offer promising candidates for optical tweezing and precision machining. Furthermore, the space-time nonseparability is expected to yield classical entanglement phenomena. The emergence of such new family of chiral SNHPs could pave the way for innovative microscopy, metrology, and telecommunication systems.

Methods

Measurement of chiral toroidal SNHPs.

The generation of chiral toroidal SNHPs was achieved using a dual-arm Archimedean spiral emitter, which consists of three main components: two radiating arms fed in phase, a dielectric substrate, and a feed structure. We measured the S_{21} parameter of the spiral emitter as the spatial channel response using an R&S®ZNA vector network analyzer, which supports a frequency range of 10 MHz to 50 GHz. For the measurement of the transversely polarized component of the chiral toroidal SNHPs, a waveguide probe antenna was used as the receiving antenna. Due to the operational bandwidth and mode of the waveguide antenna, we employed four different waveguides to cover the required frequency bands. For the measurement of the longitudinally polarized component of the chiral toroidal SNHPs, a monopole antenna was used as the receiving antenna. This antenna operates in the 1.4-10.5 GHz range, covering the necessary frequency bands for the measurements. After obtaining the spectra of the transverse and longitudinal polarization components at each frequency point, these components were synthesized with the excitation signal to reconstruct the space-time field. Detailed methods can be found in the supplementary materials.

References

- [1] Zhang, X., Liu, Y., Han, J., Kivshar, Y., & Song, Q. Chiral emission from resonant metasurfaces. *Science* **377**(6611), 1215–1218 (2022).
- [2] Hautzinger, M. P., Pan, X., Hayden, S. C., Ye, J. Y., Jiang, Q., Wilson, M. J., ... & Beard, M. C. Room-temperature spin injection across a chiral perovskite/III–V

interface. *Nature* **631**, 307–312 (2024).

[3] Chen, Y., Deng, H., Sha, X., Chen, W., Wang, R., Chen, Y. H., ... & Qiu, C. W. Observation of intrinsic chiral bound states in the continuum. *Nature* **613**(7944), 474–478 (2023).

[4] Nasari, H., Lopez-Galmiche, G., Lopez-Aviles, H. E., Schumer, A., Hassan, A. U., Zhong, Q., ... & Khajavikhan, M. Observation of chiral state transfer without encircling an exceptional point. *Nature* **605**(7909), 256–261 (2022).

[5] Han, M., Ji, J. B., Balčiūnas, T., Ueda, K., & Wörner, H. J. Attosecond circular-dichroism chronoscopy of electron vortices. *Nat. Phy.* **19**(2), 230–236 (2023).

[6] Bégin, J. L., Jain, A., Parks, A., Hufnagel, F., Corkum, P., Karimi, E., ... & Bhardwaj, R. Nonlinear helical dichroism in chiral and achiral molecules. *Nat. Photon.* **17**(1), 82–88 (2023).

[7] Ma, C., Ma, C., Liu, C., Guo, Q., Huang, C., Yao, G., ... & Liu, K. Strong chiroptical nonlinearity in coherently stacked boron nitride nanotubes. *Nat. Nanotech.* **19**, 1299–1305 (2024).

[8] Cai, J., Zhang, W., Xu, L., Hao, C., Ma, W., Sun, M., ... & Kuang, H. Polarization-sensitive optoionic membranes from chiral plasmonic nanoparticles. *Nat. Nanotech.* **17**(4), 408–416 (2022).

[9] Nishida, Y. Chiral light amplifier with pumped Weyl semimetals. *Phy. Rev. Lett.* **130**(9), 096903 (2023).

[10] Chen, W., Liu, Y., Yu, A. Z., Cao, H., Hu, W., Qiao, W., ... & Lu, Y. Q. Observation of Chiral Symmetry Breaking in Toroidal Vortices of Light. *Phy. Rev. Lett.* **132**(15),

153801 (2024).

[11] Mayer, N., Patchkovskii, S., Morales, F., Ivanov, M., & Smirnova, O. Imprinting chirality on atoms using synthetic chiral light fields. *Phys. Rev. Lett.* **129**(24), 243201 (2022).

[12] Jones, R. R., Kerr, J. F., Kwon, H., Clowes, S. R., Ji, R., Petronijevic, E., ... & Valev, V. K. Chirality conferral enables the observation of hyper-Raman optical activity. *Nat. Photon.* **18**, 982–989 (2024).

[13] Furlan, F., Moreno-Naranjo, J. M., Gasparini, N., Feldmann, S., Wade, J., & Fuchter, M. J. Chiral materials and mechanisms for circularly polarized light-emitting diodes. *Nat. Photon.* **18**, 658–668 (2024).

[14] Loetgering, L., Baluktsian, M., Keskinbora, K., Horstmeyer, R., Wilhein, T., Schütz, G., ... & Witte, S. Generation and characterization of focused helical x-ray beams. *Sci. Adv.* **6**(7), eaax8836 (2020).

[15] Cruz-Delgado, D., Yerolatsitis, S., Fontaine, N. K., Christodoulides, D. N., Amezcua-Correa, R., & Bandres, M. A. Synthesis of ultrafast wavepackets with tailored spatiotemporal properties. *Nat. Photon.* **16**(10), 686–691 (2022).

[16] Chen, L., Zhu, W., Huo, P., Song, J., Lezec, H. J., Xu, T., & Agrawal, A. Synthesizing ultrafast optical pulses with arbitrary spatiotemporal control. *Sci. Adv.* **8**(43), eabq8314 (2022).

[17] Lin, Q., Feng, F., Cai, Y., Lu, X., Zeng, X., Wang, C., ... & Yuan, X. Direct space–time manipulation mechanism for spatio-temporal coupling of ultrafast light field. *Nat. Commun.* **15**(1), 2416 (2024).

- [18] Piccardo, M., de Oliveira, M., Policht, V. R., Russo, M., Ardini, B., Corti, M., ... & Ambrosio, A. Broadband control of topological–spectral correlations in space–time beams. *Nat. Photon.* **17**(9), 822–828 (2023).
- [19] Chen, B., Zhou, Y., Liu, Y., Ye, C., Cao, Q., Huang, P., ... & Liu, J. Integrated optical vortex microcomb. *Nat. Photon.* **18**, 625–631 (2024).
- [20] Liu, Y., Lao, C., Wang, M., Cheng, Y., Wang, Y., Fu, S., ... & Yang, Q. F. Integrated vortex soliton microcombs. *Nat. Photon.* **18**, 632–637 (2024).
- [21] Kaelberer, T., Fedotov, V. A., Papasimakis, N., Tsai, D. P. & Zheludev, N. I. Toroidal dipole response in a metamaterial. *Science* **10**, 1510–1512 (2010).
- [22] Zdagkas, A., McDonnell, C., Deng, J., Shen, Y., Li, G., Ellenbogen, T., ... & Zheludev, N. I. Observation of toroidal pulses of light. *Nat. Photon.* **16**(7), 523–528 (2022).
- [23] Papasimakis, N., Fedotov, V. A., Savinov, V., Raybould, T. A. & Zheludev, N. I. Electromagnetic toroidal excitations in matter and free space. *Nat. Mater.* **15**, 263–271 (2016).
- [24] Kuprov, I., Wilkowski, D., & Zheludev, N. Toroidal optical transitions in hydrogen-like atoms. *Sci. Adv.* **8**(45), eabq6751(2022).
- [25] Miroshnichenko, A. E. et al. Nonradiating anapole modes in dielectric nanoparticles. *Nat. Commun.* **6**, 8069 (2015).
- [26] Shen, Y., Hou, Y., Papasimakis, N., & Zheludev, N. I. Supertoroidal light pulses as electromagnetic skyrmions propagating in free space. *Nat. Commun.* **12**(1), 5891 (2021).

- [27] Shen, Y., Papasimakis, N., & Zheludev, N. I. Nondiffracting supertoroidal pulses: optical “Kármán vortex streets”. *Nat. Commun.* **15**(1), 4863 (2024).
- [28] Shen, Y. & Rosales-Guzmán, C. Nonseparable states of light: from quantum to classical. *Laser Photon. Rev.* **16**(7), 2100533 (2022).
- [29] Shen, Y., Zdagkas, A., Papasimakis, N., & Zheludev, N. I. Measures of space-time nonseparability of electromagnetic pulses. *Phy. Rev. Res.* **3**(1), 013236 (2021).
- [30] Raybould, T., Fedotov, V. A., Papasimakis, N., Youngs, I., & Zheludev, N. I. Exciting dynamic anapoles with electromagnetic doughnut pulses. *Appl. Phys. Lett.* **111**(8), 081104 (2017).
- [31] Jana, K., Mi, Y., Møller, S. H., Ko, D. H., Gholam-Mirzaei, S., Abdollahpour, D., ... & Corkum, P. B. Quantum control of flying doughnut terahertz pulses. *Sci. Adv.* **10**(2), ead11803 (2024).
- [32] Wang, R., Bao, P. Y., Hu, Z. Q., Shi, S., Wang, B. Z., Zheludev, N. I., & Shen, Y. Observation of resilient propagation and free-space skyrmions in toroidal electromagnetic pulses. *Appl. Phys. Rev.* **11**, 031411 (2024).
- [33] Wang, R., Bao, P. Y., Hu, Z. Q., Wang, B. Z., & Shen, Y. Single-antenna super-resolution positioning with nonseparable toroidal pulses, *Commun. Phys.* **7**, 356 (2024).
- [34] Ziolkowski, R. W. Exact solutions of the wave equation with complex source locations. *Journal of Mathematical Physics* **26**(4), 861–863(1985).
- [35] Ziolkowski, R. W. Localized transmission of electromagnetic energy. *Phy. Rev. A* **39**(4), 2005 (1989).
- [36] Hellwarth, R. W., & Nouchi, P. Focused one-cycle electromagnetic pulses. *Phy.*

Rev. E **54**(1), 889 (1996).

[37] Lekner, J. Localized electromagnetic pulses with azimuthal dependence. *Journal of Optics A: Pure and Applied Optics* **6**(7), 711 (2004).

[38] Lekner, J. Helical light pulses. *Journal of Optics A: Pure and Applied Optics* **6**(10), L29 (2004).

[39] Shi, S., Wang, r., Xiong, M., Zhou, Q., Wang, B. Z., & Shen, Y. Double-helix singularity and vortex–antivortex annihilation in space-time helical pulses. *Nanophotonics*, 0480 (2024)

[40] Rungta, P., Bužek, V., Caves, C. M., Hillery, M., & Milburn, G. J., Universal state inversion and concurrence in arbitrary dimensions, *Phys. Rev. A* **64**, 042315 (2001).

[41] James, D. F. V., Kwiat, P. G., Munro, W. J., & White, A. G., On the measurement of qubits, in *Asymptotic Theory of Quantum Statistical Inference: Selected Papers* (World Scientific, Singapore, 2005), pp. 509–538.

[42] Spektor, G. , Kilbane, D. , Mahro, A. K. , Frank, B. , Ristok, S. , & Gal, L. , et al. Revealing the subfemtosecond dynamics of orbital angular momentum in nanoplasmonic vortices. *Science* **355**(6330), 1187–1191 (2017).

[43] Dai, Y. , Zhou, Z. , Ghosh, A. , Mong, R. S. K. , Kubo, A. , & Huang, C. B. , et al. Plasmonic topological quasiparticle on the nanometre and femtosecond scales. *Nature* **588**, 616–619 (2020).

[44] Frischwasser, K. , Cohen, K. , Kher-Alden, J. , Dolev, S. , & Bartal, G. Real-time sub-wavelength imaging of surface waves with nonlinear near-field optical microscopy. *Nat. Photon.* **442**, 442–448 (2021).

- [45] Ni, J. , Huang, C. , Zhou, L. M. , Gu, M. , Song, Q. , & Kivshar, Y. , et al. Multidimensional phase singularities in nanophotonics. *Science* **374**(6566), eabj0039 (2021).
- [46] Deng, Z. L. , Shi, T. , Krasnok, A. , Li, X. , & Alù, Andrea. Observation of localized magnetic plasmon skyrmions. *Nat. Commun.* **13**, 8, (2022).
- [47] Fanciulli, M. , Pancaldi, M. , Pedersoli, E. , Vimal, M. , Bresteau, D. , & Luttmann, M. , et al. Observation of magnetic helicoidal dichroism with extreme ultraviolet light vortices. *Phy. Rev. Lett.* **128**(7), 077401 (2022).
- [48] Wu, C. , Kumar, S. , Kan, Y. , Komisar, D. , Wang, Z. , & Bozhevolnyi, S. , et al. Room-temperature on-chip orbital angular momentum single-photon sources. *Sci. Adv.* **8**, eabk3075 (2022).

Acknowledgments

This work has been supported by the National Natural Science Foundation of China (62171081, 61901086, U2341207), the Natural Science Foundation of Sichuan Province (2022NSFSC0039), the Aeronautical Science Foundation of China (2023Z062080002), European Research Council (FLEET-786851), Singapore Ministry of Education (MOE) AcRF Tier 1 grant (RG157/23, RT11/23). Y. S. also acknowledges the support from Nanyang Technological University Start Up Grant. M.A.P. acknowledges support from the Spanish Ministry of Science and Innovation, Gobierno de España, under Contract No. PID2021-122711NB-C21. The optical experiments presented in this paper were conducted by Y. S. under the supervision of

Prof. Nikolay I. Zheludev and Nikitas Papisimakis at the Optoelectronics Research Centre, University of Southampton. We extend our sincere gratitude to them for their guidance and support.

Author contributions

R.W. and Y.S. conceived the ideas and supervised the project, R.W., Y.S., S.S. and Z.Z. performed the theoretical modeling and numerical simulations, R.W. and Y.S. developed the experimental methods, R.W., Y.S., S.S. and Z.Z. conducted the experimental measurements, R.W., Y.S., B.Z.W., M. A. P. and N.M.C. conducted data analysis. All authors wrote the manuscript and participated the discussions.

Competing interests

The authors declare no competing financial interests.

Data and materials availability

The data that support the findings of this study are available from the corresponding author upon reasonable request.

Additional information

Supplementary information is available for this paper. Correspondence and requests for materials should be addressed to R.W. and Y.S..

Figures

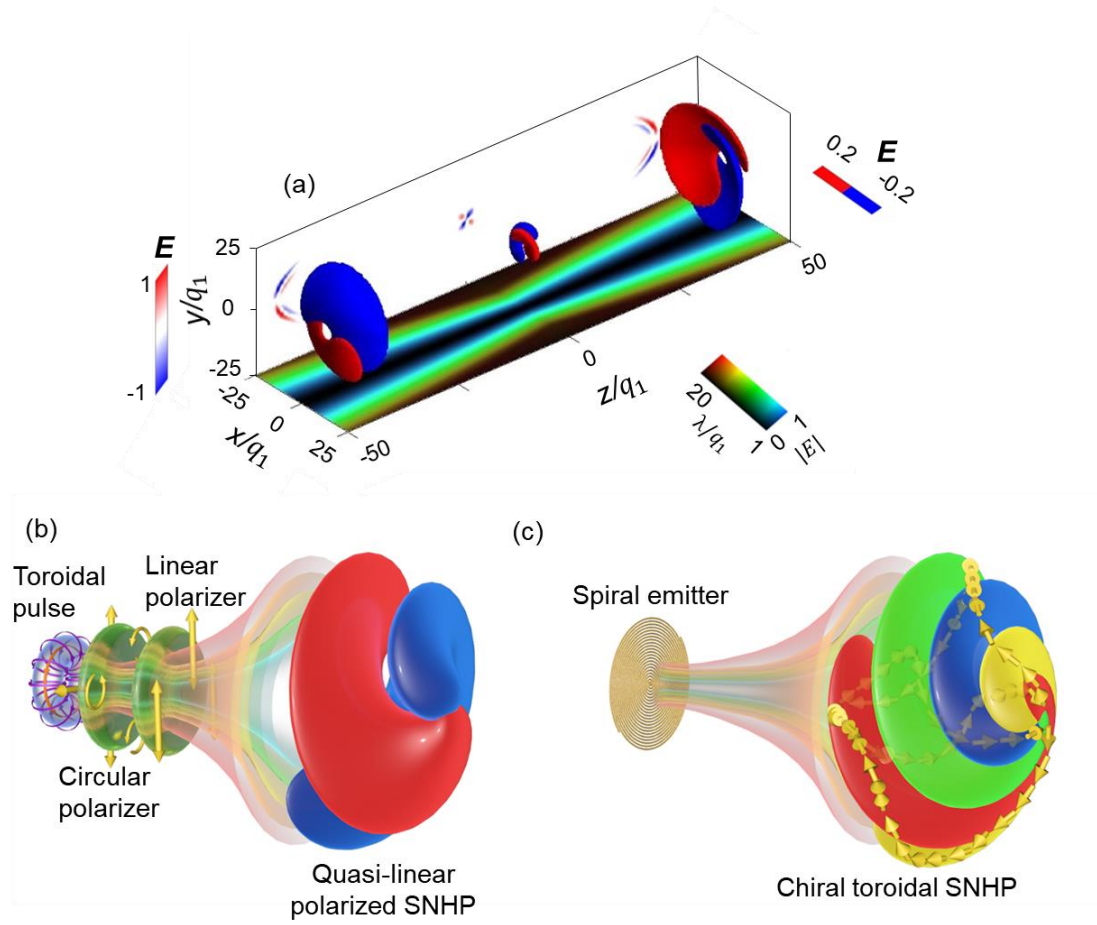


Fig. 1. Characteristics of SNHPs and blueprint for their generation. (a) Spatiotemporal structure and propagation of the SNHP. The electric field of the SNHP with $\ell=1$ consists of two helical lobes, lasting for a single cycle. The frequency and intensity in xz plane are represented by colour and brightness, respectively. The position-dependent frequency is across the transverse plane: lower-frequency components dominate at the periphery of the pulse, while higher frequencies are more prevalent at its central region, indicating isodiffraction propagation. (b) Schematic of the generation of quasi-linearly polarized optical SNHPs. The transverse electric field component of the TM optical toroidal pulse is first decomposed into circularly polarized

fields using a circular polarizer and then further decomposed into a quasi-linearly polarized SNHP using a linear polarizer. The blue and red lobes represent positive and negative electric field components, respectively. (c) Schematic of the generation of chiral toroidal microwave SNHPs. A dual-arm spiral antenna directly emits SNHPs, which exhibit both transverse and longitudinal components. The blue and red lobes denote the positive and negative components, respectively, of the vertically polarized transverse electric field. Similarly, the yellow and green lobes represent the positive and negative components, respectively, of the horizontally polarized transverse electric field. The three-dimensional electric field vectors form a chiral toroidal helical topology.

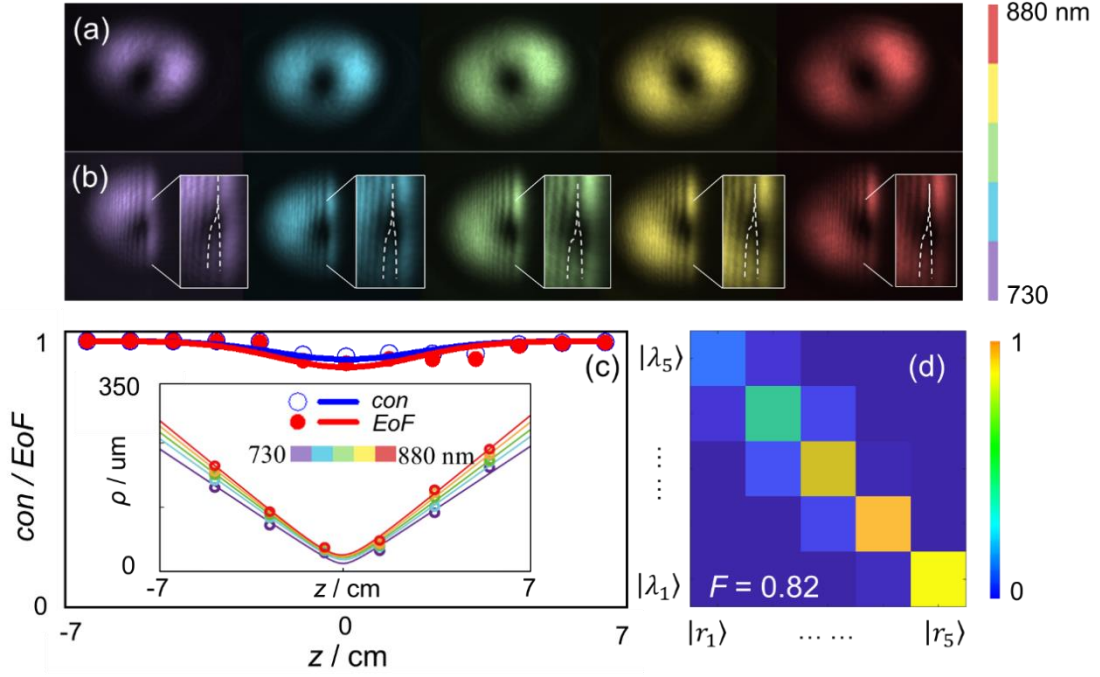


Fig. 2. The scheme and spectrum of generated optical quasi-linearly polarized SNHPs. The intensity distributions of light detected by CCD camera at different wavelengths in the absence and presence of an opaque edge are shown in (a) and (b), respectively. The ring-shaped intensity and fork-shaped pattern indicate the presence of optical vortices, consistent with those of SNHPs. The concurrence and entanglement of formation evolution of the measured transverse electric field components in (c) indicate the generated SNHPs have a good space-time nonseparability. The inserted figure in (c) represents the measured tracking curves of the maximum field positions for different wavelengths. The trajectories of different wavelengths do not cross when the incident wave is a toroidal pulse, demonstrating isodiffraction characteristics. State-tomography matrix of generated pulses when the incident wave is a toroidal pulse is shown in (d). When the incident wave is a toroidal pulse, the diagonalized matrix visually demonstrates isodiffraction characteristics. The measured fidelity is 0.82, indicating a good match with canonical SNHPs.

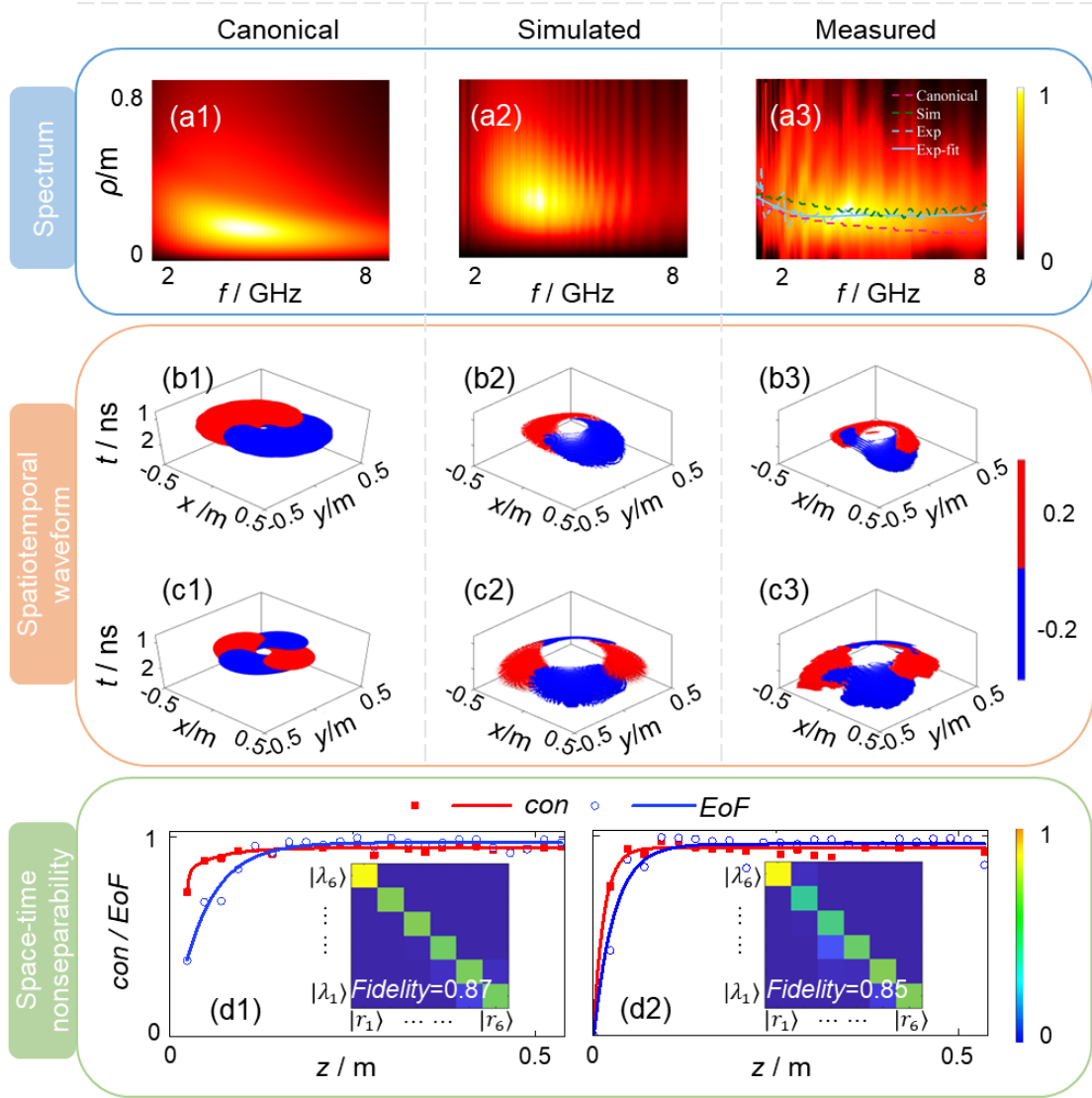


Fig. 3. The spatio-spectral and spatiotemporal structure of generated microwave chiral toroidal SNHPs. Spatial frequency spectra at $z=0.4$ m of (a1) canonical, (a2) simulated, and (a3) measured transverse component E_y of the SNHPs with parameters $q_1 = 0.03$ m, $q_2 = 20q_1$, and $\ell=1$. The maximum positions of each frequency point corresponding to canonical, simulated, and measured SNHPs are highlighted in (a3). SNHPs exhibit a wide bandwidth, spatial spectra narrow as the frequency increases, and the spectrum maximum moving closer to the central axis $\rho = 0$. Spatiotemporal field distributions of the transverse component E_y and longitudinal component E_z for

the canonical, simulated, and measured SNHPs are shown in (b1-b3) and (c1-c3), respectively. Both simulated and measured E_y components exhibit a double-lobe single-cycle helical topology and E_z components display a four-lobe helical topology, akin to the canonical SNHPs. The concurrence and entanglement of formation evolution of the measured transverse electric field components (d1) E_x and (d2) E_y after radiating from the spiral emitter indicates the generated SNHPs evolve towards stronger space-time nonseparability during propagation. The state-tomography matrix of E_x and E_y of the generated chiral toroidal SNHPs are inserted in (d1) and (d2), respectively. The measured fidelities exceed 0.8, suggesting a relatively good match with canonical chiral toroidal SNHPs.